Analytical travelling vortex solutions of hyperbolic equations for validating very high order schemes

Mario Ricchiuto[*] and Davide Torlo[†]

September 21, 2021

Abstract

Testing the order of accuracy of (very) high order methods for shallow water (and Euler) equations is a delicate operation and the test cases are the crucial starting point of this operation. We provide a short derivation of vortex-like analytical solutions in 2 dimensions for the shallow water equations (and, hence, Euler equations) that can be used to test the order of accuracy of numerical methods. These solutions have different smoothness in their derivatives (up to $\mathcal{C}^\infty$) and can be used accordingly to the order of accuracy of the scheme to test.

1 Moving vortex solutions and regularity requirements

1.1 Shallow water equations and moving profiles

We consider the shallow water equations (SWEs) on a flat bathymetry reading

$$\begin{cases} \partial_t h & +\nabla \cdot (h\vec{u}) = 0, \\ \partial_t (h\vec{u}) & +\nabla \cdot (h\vec{u} \otimes \vec{u}) + gh\nabla h = 0, \end{cases} \tag{1}$$

$h : \mathbb{R}^2 \to \mathbb{R}^+$, $\vec{u} : \mathbb{R}^2 \to \mathbb{R}^2$, $g \in \mathbb{R}^+$.
Following [6] we consider solutions of the form $h = H_0(\vec{\zeta})$ and $\vec{u} = \vec{u}_\infty + \vec{U}_0(\vec{\zeta})$, with $\zeta = \vec{x} - \vec{u}_\infty t$, and $\vec{u}_\infty$ constant. Replacing in the SWEs we obtain

$$\begin{cases} \vec{U}_0 \cdot \nabla_{\vec{\zeta}} H_0 & +H_0 \nabla_{\vec{\zeta}} \cdot \vec{U}_0 = 0, \\ \vec{U}_0 \cdot \nabla_{\vec{\zeta}} \vec{U}_0 & +\nabla_{\vec{\zeta}} H_0 = 0, \end{cases} \tag{2}$$

which justifies looking for stationary solutions with solenoidal velocity fields with depth variations uniquely in the cross-stream direction. These conditions are easily met for solutions with cylindrical symmetry.

1.2 SWEs in cylindrical coordinates

We consider cylindrical coordinates defined in 2D by the distance from the origin $r^2 = x^2 + y^2$, and the counter-clockwise angle θ measured from the positive x axis so that

$$x = r\cos\theta , \;\; y = r\sin\theta. \tag{3}$$

---

[*]Team CARDAMOM, Inria Bordeaux Sud-Ouest, - 200 av. de la vieille tour, 33405 Talence, France
[†]Team CARDAMOM, Inria Bordeaux Sud-Ouest, - 200 av. de la vieille tour, 33405 Talence, France

1

We also introduce the direction vectors $\hat{r} = (\cos\theta, \sin\theta)$, and $\hat{r}^{\perp} = (-\sin\theta, \cos\theta)$. This notation can be used to write the shallow water equations in polar coordinates as

$$
\begin{cases}
\partial_t h & +\partial_r(hu_r) + \dfrac{1}{r}\left(\partial_\theta(hu_\theta) + hu_r\right) = 0 \\[2mm]
\partial_t(hu_r) & +\partial_r(hu_r^2) + gh\partial_r h + \dfrac{1}{r}\left(\partial_\theta(hu_r u_\theta) + h(u_r^2 - u_\theta^2)\right) = 0 \\[2mm]
\partial_t(hu_\theta) & +\partial_r(hu_r u_\theta) + \dfrac{1}{r}\left(gh\partial_\theta h + \partial_\theta(hu_\theta^2) + 2hu_r u_\theta\right) = 0
\end{cases}
\tag{4}
$$

where

$$
\begin{aligned}
u_r = \vec{u}\cdot\hat{r} = \cos(\theta)u_x + \sin(\theta)u_y\,, \quad u_\theta = \vec{u}\cdot\hat{r}^{\perp} = -\sin(\theta)u_x + \cos(\theta)u_y, \\
u_x = \cos(\theta)u_r - \sin(\theta)u_\theta\,, \quad u_y = \sin(\theta)u_r + \cos(\theta)u_\theta.
\end{aligned}
\tag{5}
$$

1.3 Stationary vortex ODE

To mimic (2), we consider the particular case with all zero time derivatives and only radial velocity, i.e.,

$$
\begin{aligned}
\partial_t h &= 0, \\
\partial_t u_r &= \partial_t u_\theta = 0, \\
h &= h(r)\,, \quad \partial_\theta h = 0, \\
u_\theta &= u_\theta(r)\,, \quad \partial_\theta u_\theta = 0, \\
u_r &= 0.
\end{aligned}
\tag{6}
$$

With the above hypotheses we can readily check that the first and the last in (4) are identically satisfied, while the second reduces to

$$
h'(r) = \frac{u_\theta^2}{gr}.
\tag{7}
$$

Assuming further that $u_\theta = \omega(r)r$ we end up with

$$
h'(r) = \frac{r\omega^2(r)}{g}.
\tag{8}
$$

Given a law for the angular velocity ω this ODE can be integrated to obtain closed form expressions for the depth and, conversely, given a law for h, u_θ and ω can be obtained differentiating h.

1.4 Regularity requirements for validating high order methods

To validate higher order methods, exact solutions of the shallow water system should have enough regularity to allow the validity of high order approximation results. The classical interpolation estimate for finite element approximations [3, §1.5] for a function with $\partial_\alpha v \in L^p(\Omega)$, for a multi-index $|\alpha| \leq l+1$, is the following

$$
\|v - v_h\|_{L^p(\Omega)} \leq ch^{l+1}|v|_{l+1, L^p(\Omega)},
\tag{9}
$$

with h the mesh size. This means that to benchmark an $l+1$ order accurate method, we need an exact solution with integrable $l+1$ derivatives. In practice, for a system different variables may have different regularity. This may lead in practice to convergence rates somewhat in between those of the different variables, depending on how the error is defined and measured.

1.5 Extension to Euler equations

Similarly to SWEs other moving vortexes can solve exactly Euler equations. They read

$$
\begin{cases}
\partial_t \rho & +\partial_x(\rho u_x) + \partial_y(\rho u_y) = 0, \\
\partial_t(\rho u_x) & +\partial_x(\rho u_x^2 + p) + \partial_y(\rho u_x u_y) = 0, \\
\partial_t(\rho u_y) & +\partial_x(\rho u_x u_y) + \partial_y(\rho u_y^2 + p) = 0, \\
\partial_t(\rho E) & +\partial_x[u_x(\rho E + p)] + \partial_y[u_y(\rho E + p)] = 0,
\end{cases}
\tag{10}
$$

where the perfect gas equation of state closes the system, i.e.,

$$
\rho E = \frac{p}{\gamma - 1} + \frac{1}{2}\rho(u_x^2 + u_y^2).
\tag{11}
$$

Here $\gamma \in \mathbb{R}^+$ is the adiabatic constant. Equivalently, we can write Euler equations in polar coordinates

$$
\begin{cases}
\partial_t \rho & +\frac{1}{r}\partial_r(r\rho u_r) + \frac{1}{r}\partial_\theta(\rho u_\theta) = 0, \\
\partial_t(\rho u_r) & +\frac{1}{r}\partial_r(r(\rho u_r^2 + p)) + \frac{1}{r}\partial_\theta(\rho u_r u_\theta) - \frac{1}{r}(\rho u_\theta^2 + p) = 0, \\
\partial_t(\rho u_\theta) & +\frac{1}{r}\partial_r(r\rho u_r u_\theta) + \frac{1}{r}\partial_\theta(\rho u_\theta^2 + p) + \frac{1}{r}\rho u_\theta u_r = 0, \\
\partial_t(\rho E) & +\frac{1}{r}\partial_r[r u_r(\rho E + p)] + \frac{1}{r}\partial_\theta[u_\theta(\rho E + p)] = 0.
\end{cases}
\tag{12}
$$

Using the vortex form (6), we have that u_r is set to 0 and ∂_θ is equal to 0 for all the unknowns. Hence, the system reduces for steady vortexes to

$$
r\partial_r p = \rho u_\theta^2.
\tag{13}
$$

This form can be easily solved in two situations.

Isentropic case

The isentropic case ($S = p/\rho^\gamma =$ constant) for $\gamma > 1$ leads to

$$
\frac{\gamma}{\gamma - 1}\partial_r(\rho^{\gamma-1}) = \frac{u_\theta^2}{r}.
\tag{14}
$$

Following the approach of (7), if we define any angular velocity $\omega(r)$ and consequentially

$$
u_r = 0, \qquad u_\theta(r) := r\omega(r), \qquad \rho(r) := \left(\rho_0 + \int \frac{\gamma - 1}{\gamma} r\omega^2(r)dr\right)^{\frac{1}{\gamma-1}}, \qquad p = \rho^\gamma,
\tag{15}
$$

where with the integral is meant up to a constant, that can be set with ρ at $r = \infty$. Clearly, this formulation is equivalent to the SWE ones setting $\gamma = 2$ and $g = 2$, and all the following derivation can be used in Euler equations.

Isochoric vortex

The second option to obtain a steady vortex is to set a constant density $\rho(r) = \rho_0$, and (13) becomes a differential equation for p. Again, we obtain

$$
u_r = 0, \qquad u_\theta(r) := r\omega(r), \qquad \rho(r) = \rho_0, \qquad p(r) := \int \rho_0 r\omega^2(r)dr.
\tag{16}
$$

3

N	Error h	Order h	Error u	Order u	Error v	Order v
8	2.755e-04	0.000	3.072e-03	0.000	3.072e-03	0.000
16	1.650e-04	0.739	8.940e-04	1.781	8.938e-04	1.781
32	3.039e-05	2.441	1.654e-04	2.434	1.654e-04	2.434
64	4.188e-06	2.859	3.568e-05	2.213	3.568e-05	2.213
128	5.018e-07	3.061	7.879e-06	2.179	7.879e-06	2.179
256	5.755e-08	3.124	1.588e-06	2.311	1.588e-06	2.311
512	6.320e-09	3.187	2.970e-07	2.418	2.970e-07	2.418

Table 1: Order of convergence for (19) obtained with WENO5 on a cartesian grid with $N \times N$ cells

2 The vortex solution of [6]

The following is an example often used in literature obtained by setting

$$\omega(r) = \begin{cases} \Gamma(1 + \cos(\pi \dfrac{r}{r_0})) & \text{if } r \leq r_0, \\ 0 & \text{otherwise.} \end{cases} \tag{17}$$

This expression can be fed into (8) and integrated backwards from $r = r_0$ to r with initial condition $h = h_0$ to obtain

$$h = h_0 - \frac{\Gamma^2 r_0^2}{g\pi^2} \begin{cases} H(\pi) - H(\pi \dfrac{r}{r_0}) & \text{if } r \leq r_0, \\ 0 & \text{otherwise,} \end{cases} \tag{18}$$

with

$$H(x) = 2\cos x + 2x \sin x + \frac{\cos(2x)}{8} + \frac{x \sin(2x)}{4} + \frac{12x^2}{16}. \tag{19}$$

Note that

$$\begin{aligned} H'(\pi) &= 0 , \ u'_\theta(\pi) = 0, \\ H^{(2)}(\pi) &= 0 , \ u^{(2)}_\theta(\pi) = \pi \neq 0, \\ H^{(3)}(\pi) &= 0 , \ u^{(3)}_\theta(\pi) \neq 0, \\ H^{(4)}(\pi) &= 0 , \ u^{(4)}_\theta(\pi) \neq 0, \\ H^{(5)}(x) &= 6\pi \neq 0 , \ u^{(5)}_\theta(\pi) \neq 0. \end{aligned} \tag{20}$$

According to (9) this solution should allow to obtain at most second order of accuracy, due to the limited regularity of the velocity. In practice, some computations have shown a little extra convergence for the depth, for which, at least on relatively coarse resolutions, one can manage to obtain toughly third order convergence. The convergence study obtained with a WENO5 on Cartesian grids on $[0, 1]^2$ with a RK(6,5) is shown in table 1. The tests are run on the vortex defined with $r_0 = 0.25$ and centered in $(0.5, 0.5)$, $h_0 = 1$ and Γ such that $h(0) = 0.99$. It is clear that the order of accuracy for h cannot reach 3 and that the velocities can be approximated with only order 2.

3 Non compact supported vortexes

There are many other vortexes for Euler's equation, Euler himself in [4] suggested a similar simplification to obtain a steady solution, and in 1998 Shu [7] proposed a vortex to study the accuracy of WENO5

schemes from a qualitatively point of view. In the following years, this tests and some modifications of it became a real benchmark for testing the accuracy of many schemes [5, 10, 9, 1, 2]. The main idea follows form the definition of a vortex where the base function $\omega(r)$ is a Gaussian function $\omega(r) = \Gamma e^{-(r/r_0)^2}$, where r_0 is a rescaling factor for the width and Γ rescales the amplitude. Despite being the benchmark test for many problems, this test does not have a compact support and boundaries are a real issue, in particular when dealing with very high order of accuracy methods, as shown, for instance, in [8]. Nevertheless, it was often used with periodic boundary conditions even with nonzero background speed. This leads to traveling discontinuities (on the derivatives) from the boundaries to all over the domain. The techniques to *cure* this issue were various starting from enlarging the domain (or equivalently reducing r_0) to treating with nonperiodic boundary conditions (inflow/outflow with steady vortex). Of course increasing the domain means that the computational costs increase too and using inflow/outflow does not allow to make the vortex travel outside the domain.

We can easily compute

$$\begin{cases} \omega(r) = \Gamma e^{-(r/r_0)^2} \\ u_\theta(r) = r\omega(r) \\ h(r) = h_0 - \frac{\Gamma^2 r_0^2}{4g} e^{-2(r/r_0)^2} = h_0 - \frac{r_0^2}{4g}\omega^2(r). \end{cases} \tag{21}$$

We plot the profile of $h(r)$ and $u_\theta(r)$ for $h_0 = 1$, Γ such that $h(0) = 0.99$ and different r_0 in figs. 1 and 2.

On the pictures one finds also the values of the maximum absolute values of the derivatives and the values of speed and height at $r = 1$. As one can see, increasing r_0 the derivatives decrease, but the values at $r = 1$ are diverging from h_0 for h and 0 for u_θ. This means that boundary effects might disturb the convergence process. For the numerical part, we will test only $r_0 = 0.2, 0.3, 0.4$, as all the other parameters leads to either very high derivatives or boundary effects. This is also visible in these tests, but this is the range where they are more bounded.

4 Compact supported traveling vortexes of arbitrary smoothness

4.1 Iterative correction of the RB-vortex to obtain arbitrary smoothness

In order to obtain more regularity in the vortex, and to be able to test higher order accuracy methods, we can generalize the previous solution. We remark that for $r/r_0 \leq 1$ (17) is equivalent to

$$\omega = \Gamma\left(1 + \cos(\rho)\right) = 2\Gamma\cos^2\left(\rho/2\right), \quad \rho = \pi\frac{r}{r_0}. \tag{22}$$

A natural way to improve the regularity of this definition for $\rho = \pi$ is to increase the exponent of the cosinus. So we look into definitions of the type

$$\omega = 2^p\Gamma\cos^{2p}\left(\rho/2\right) = \Gamma(1 + \cos\rho)^p, \quad p \geq 1 \tag{23}$$

which allows to increase the regularity, keeping bounded values of the $(p+2)$th derivative.

In practice, we need to integrate the ODE

$$h'(r) = \frac{4^p\Gamma^2}{g} r\, \cos^{4p}(\pi\frac{r}{2r_0}), \quad r \in [0, r_0], \tag{24}$$

with the condition $h(r_0) = h_0$. The solution to this problem within $[0, r_0]$ can be written as

$$h(r) = h_0 - \frac{1}{g}\left(\frac{2^p\Gamma r_0}{\pi}\right)^2 \left(H_p(\pi/2) - H_p(\rho/2)\right), \quad \rho = \pi\frac{r}{r_0}, \tag{25}$$
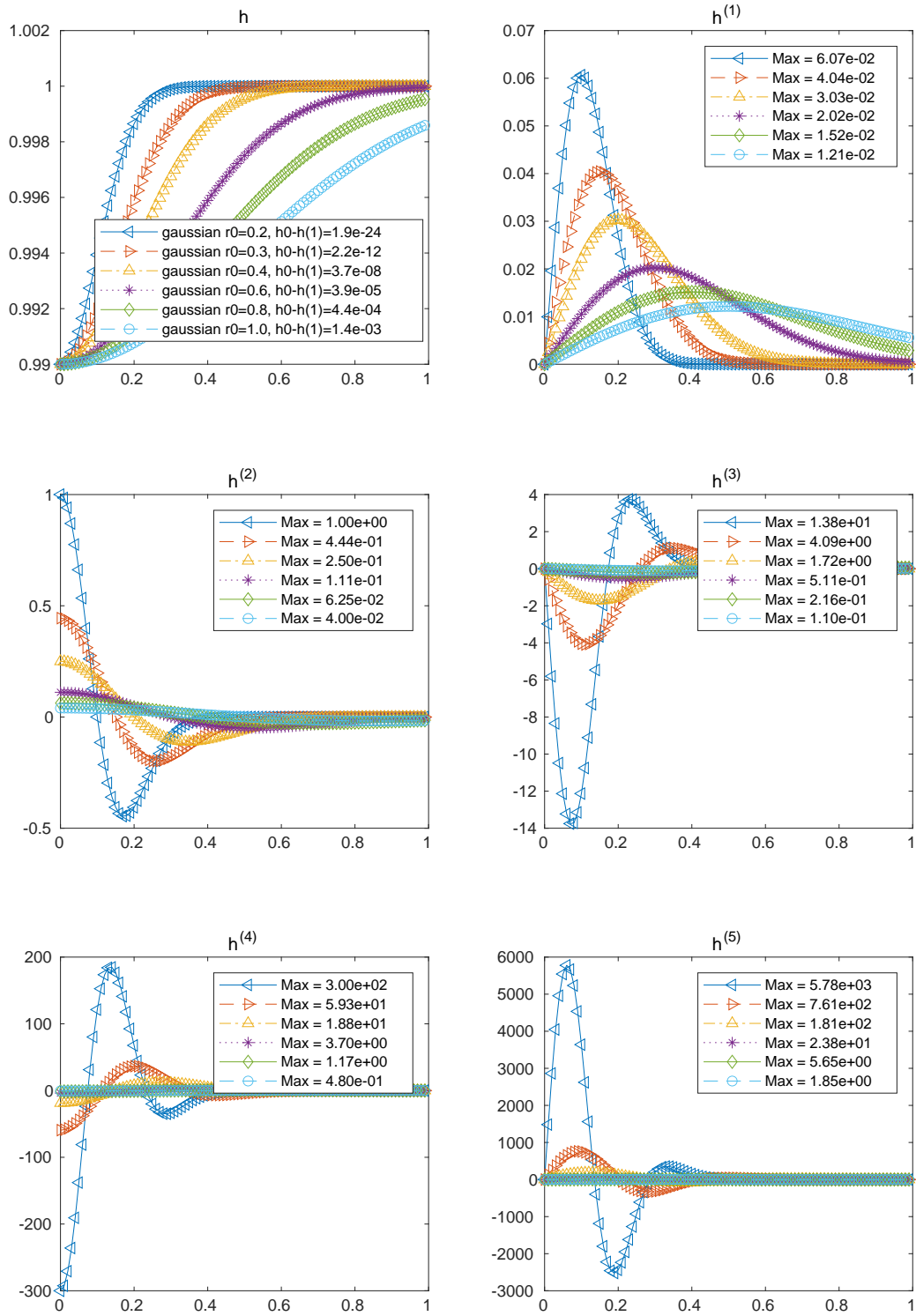
5

Figure 1: h profile and its derivatives for vortexes (21) with $r_0 = 0.2, 0.3, 0.4, 0.6, 0.8, 1$
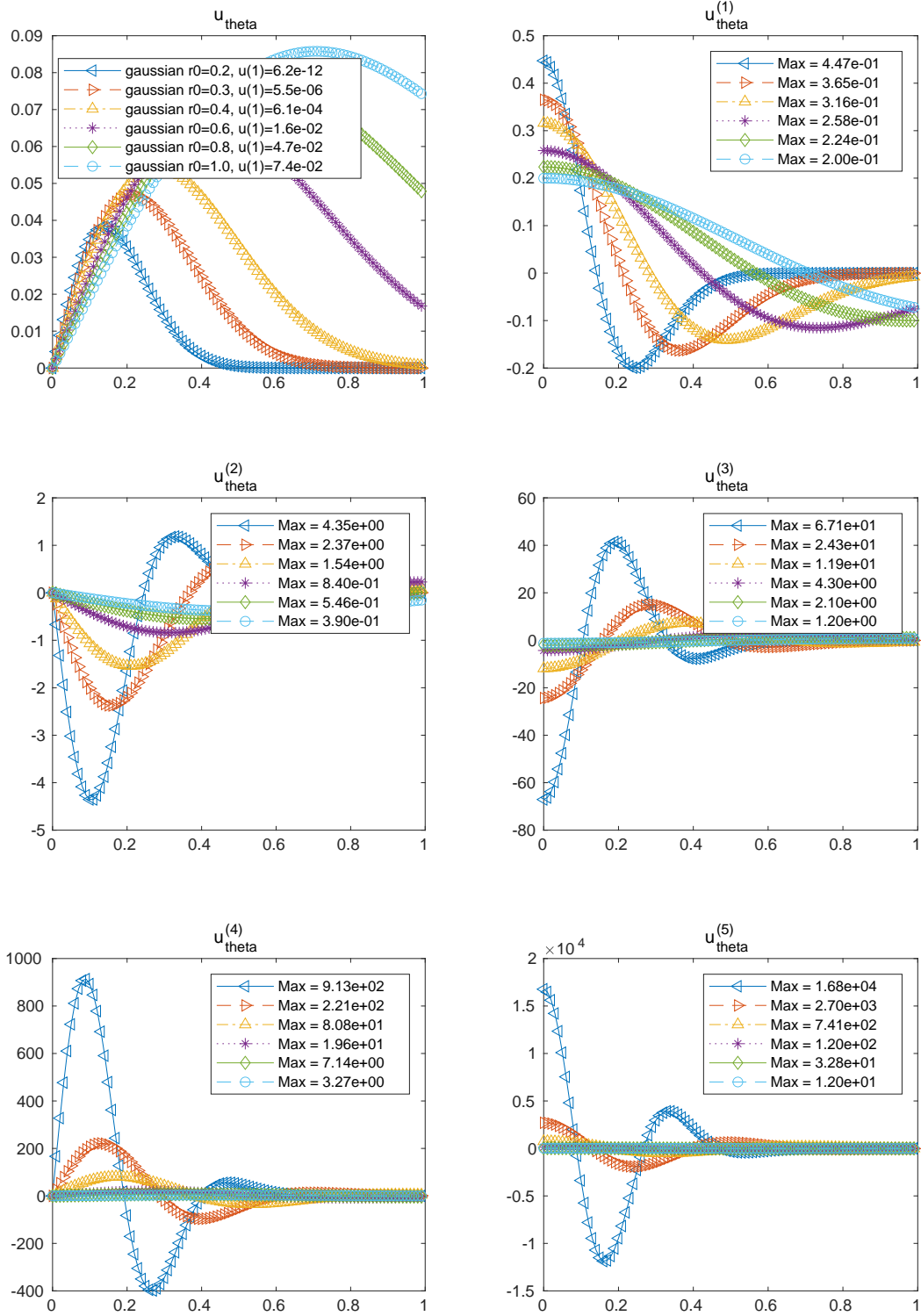
Figure 2: u_θ profile and its derivatives for vortexes (21) with $r_0 = 0.2, 0.3, 0.4, 0.6, 0.8, 1$

having set

$$H_p(x) = \int^x y \cos^{4p}(y)\, dy \tag{26}$$

up to an additional constant. Comparing to (18) we can deduce that

$$H_1(x) = \frac{1}{16} H(2x) \tag{27}$$

with $H(x)$ defined in (19). For $p > 1$ we can use the iterative integration rule

$$\int \cos^n(x)\, dx = \frac{\cos^{n-1}(x)\sin(x)}{n} + \frac{n-1}{n} \int \cos^{n-2}(x)\, dx \tag{28}$$

to show that

$$
\begin{aligned}
H_p(x) := \int x\cos^{4p}(x) &= x\int \cos^{4p}(x) - \int\int \cos^{4p}(x) \\
&= x\frac{\cos^{4p-1}(x)\sin(x)}{4p} + x\frac{4p-1}{4p}\int \cos^{4p-2}(x) - \int\left\{\frac{\cos^{4p-1}(x)\sin(x)}{4p} + \frac{4p-1}{4p}\int \cos^{4p-2}(x)\right\} \\
&= x\frac{\cos^{4p-1}(x)\sin(x)}{4p} - \int\frac{\cos^{4p-1}(x)\sin(x)}{4p} + \frac{4p-1}{4p}\left\{x\int \cos^{4p-2}(x) - \int\int \cos^{4p-2}(x)\right\} \\
&= x\frac{\cos^{4p-1}(x)\sin(x)}{4p} + \frac{\cos^{4p}(x)}{(4p)^2} + \\
&\quad \frac{4p-1}{4p}\left\{x\frac{\cos^{4p-3}(x)\sin(x)}{4p-2} + \cos^{4p-2}(x) + \frac{4p-3}{4p-2}\int x\cos^{4p-4}(x)\right\} \\
&= \frac{4p-1}{4p}\frac{4p-3}{4p-2}H_{p-1}(x) + x\frac{\cos^{4p-3}(x)\sin(x)}{4p}\left\{\frac{4p-1}{4p-2} + \cos^2(x)\right\} + \\
&\quad \cos^{4p-2}(x)\left\{\frac{\cos^2(x)}{(4p)^2} + \frac{4p-1}{4p(4p-2)^2}\right\}.
\end{aligned}
$$

This formula can be used to compute the exact solution iteratively for any $p \geq 1$ with initial value given by (27). In appendix A, we provide some values of H_p.

These vortexes suited for testing high order methods, as they are C^{2p}. Nevertheless, it is not recommended to use a very high p for not so high order methods. Indeed, we see that the estimation on the error (9) depends not only on the smoothness of the solution, but also on the seminorms. Essentially, if the derivatives are too large, we might need very fine meshes to reach the expected order of accuracy. To assess this information we plot for various vortexes the profile of $h(r)$ and of $u_\theta(r)$ and their derivatives (up to the 5th derivative). We fix for all the vortexes $r_0 = 1$, the values $h_0 = 1$ and $h(0) = 0.99$, by setting Γ and $g = 1$. In figs. 3 and 4 the plot related to the vortexes of type (25) for variables h and u_θ respectively.

In fig. 3 we barely see that the fifth derivative of the case $p = 1$ is not zero at $r = 1$, but we observe that the amplitude of the derivative functions increases with p, in particular the fifth derivative of $p = 5$ is 10 times larger than $p = 2$. In fig. 4 we immediately see that the second derivative of u_θ for $p = 1$ is discontinuous in $r = 1$, and the fourth derivative is discontinuous also for $p = 2$. Again, the higher we choose p the larger the derivatives become.

4.2 A few C^∞ examples

In this case we start from (8) and we reverse it to obtain a definition of the angular velocity given the depth:
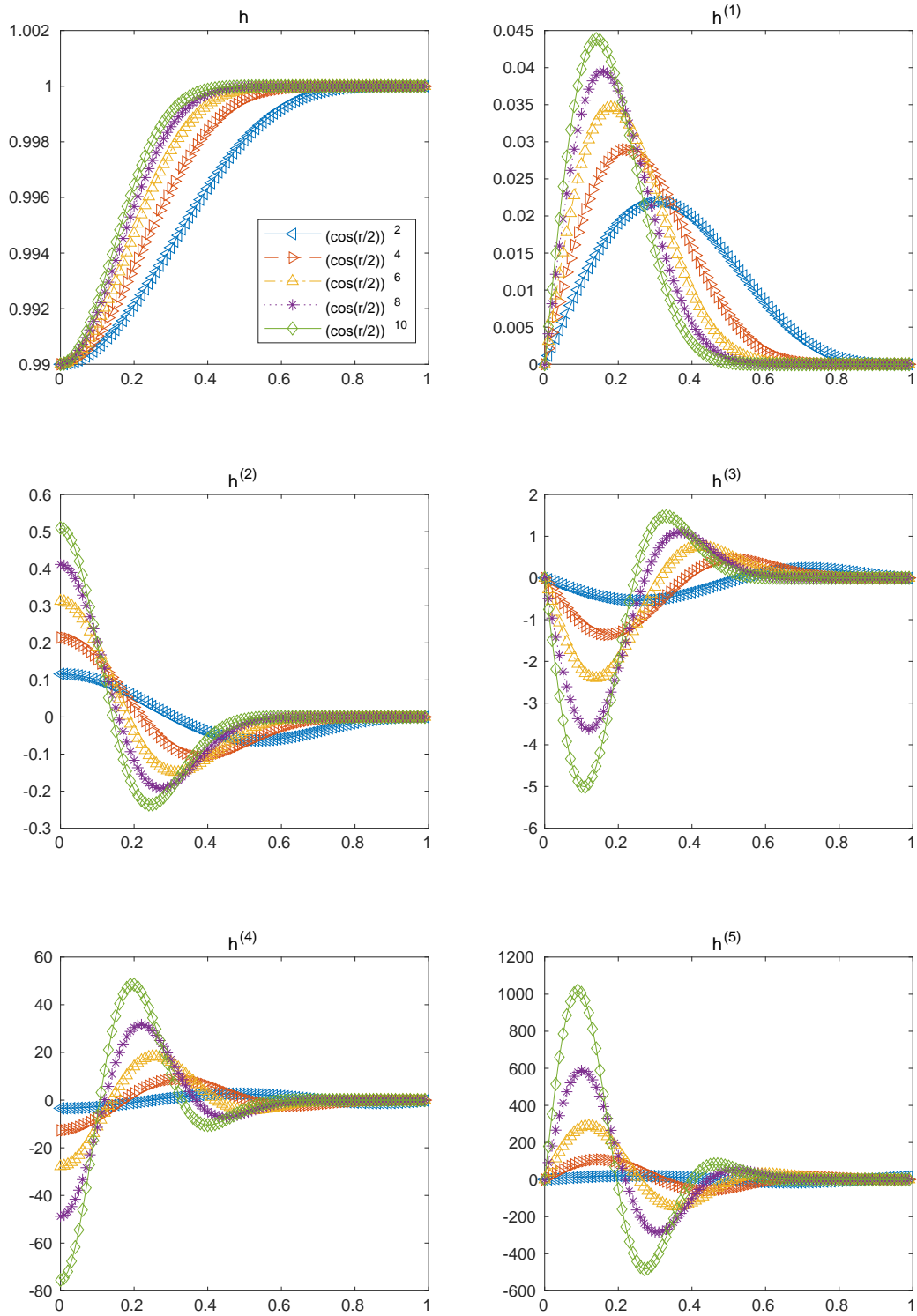
$$\omega = \sqrt{\frac{gh'}{r}}. \tag{29}$$

8

Figure 3: h profile and its derivatives for vortexes (25) with $p = 1, \ldots, 5$

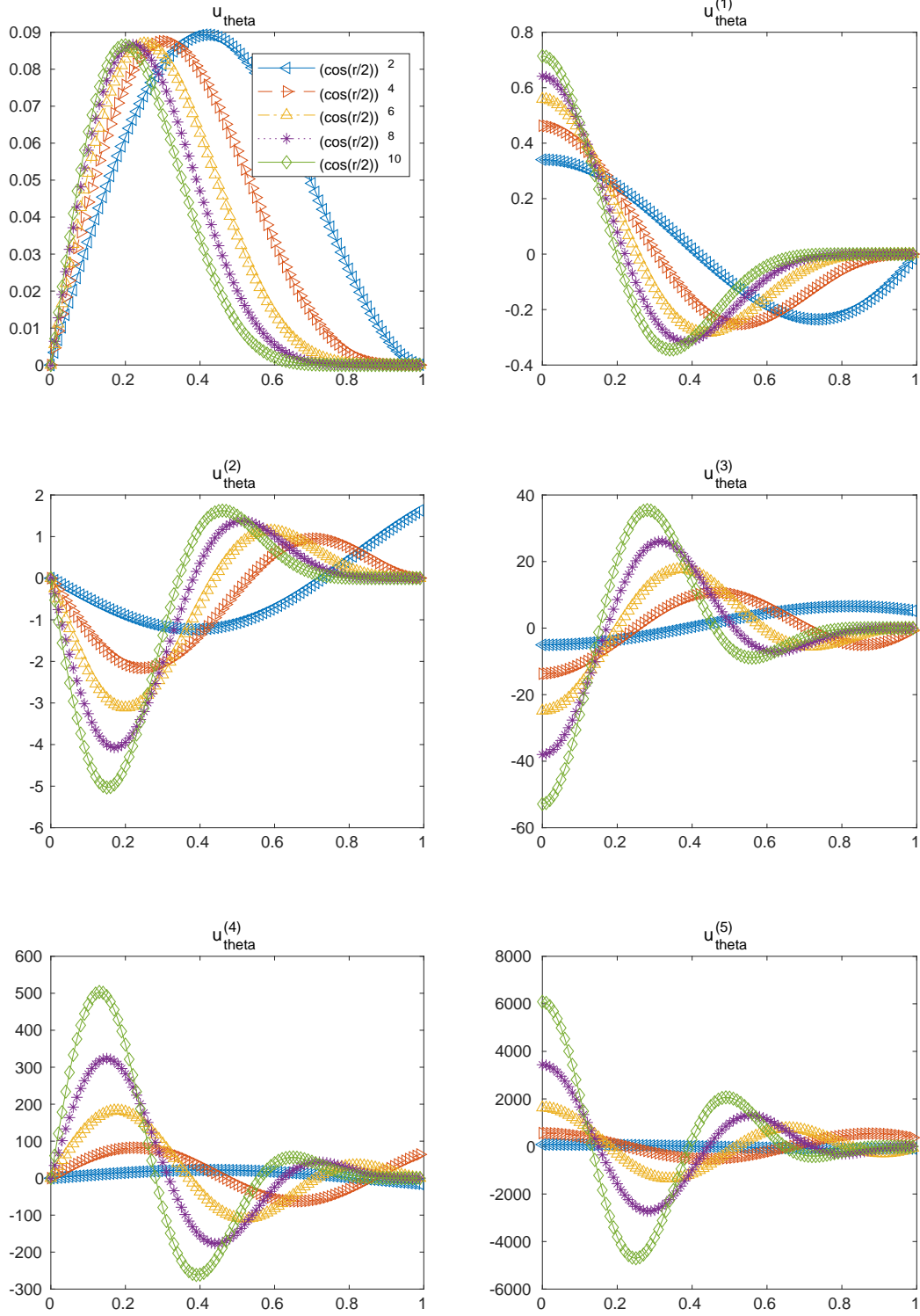Figure 4: u_θ profile and its derivatives for vortexes (25) with $p = 1, \ldots, 5$

To avoid the singularity in $r = 0$, we define the depth as a function of $\rho := (r/r_0)^2$. An example of C^∞ compactly supported function is obtained with the definition

$$h = h_0 - \Gamma^2 \begin{cases} e^{-\dfrac{1}{(1-\rho)^2}} & \text{if } \rho < 1, \\ 0 & \text{else,} \end{cases} \qquad \rho = \left(\frac{r}{r_0}\right)^2. \tag{30}$$

The angular velocity, and thus the tangential linear velocity, can be readily computed from (29):

$$\omega = \begin{cases} 2\Gamma e^{-\dfrac{1}{2(1-\rho)^2}} \sqrt{\dfrac{g}{r_0 (1-\rho)^3}} & \text{if } r < r_0, \\ 0 & \text{else,} \end{cases} \qquad \rho = \left(\frac{r}{r_0}\right)^2. \tag{31}$$

Though being C^∞, the previous function has very large derivatives and need very fine mesh to see the order of the mesh.

Alternatives could be obtained, for instance, using higher power in the exponential, for example

$$h = h_0 - \Gamma^2 \begin{cases} e^{-\dfrac{1}{(1-\rho)^p}} & \text{if } \rho < 1, \\ 0 & \text{else,} \end{cases} \qquad \rho = \left(\frac{r}{r_0}\right)^2, \tag{32}$$

leading to

$$\omega = \begin{cases} \Gamma \sqrt{\dfrac{2pg}{r_0 (1-\rho)^{p+1}}} \, e^{-\dfrac{1}{2(1-\rho)^p}} & \text{if } r < r_0, \\ 0 & \text{else,} \end{cases} \qquad \rho = \left(\frac{r}{r_0}\right)^2. \tag{33}$$

Or one can make the derivatives a bit smaller with an additional arctan function, i.e.,

$$h = h_0 - \Gamma^2 \begin{cases} e^{-\dfrac{1}{\arctan^p(1-\rho)}} & \text{if } \rho < 1, \\ 0 & \text{else,} \end{cases} \qquad \rho = \left(\frac{r}{r_0}\right)^2, \tag{34}$$

leading to

$$\omega = \begin{cases} \Gamma e^{-\dfrac{1}{2\arctan(1-\rho)^p}} \sqrt{\dfrac{2pg}{r_0 \arctan^{p+1}(1-\rho)} \dfrac{1}{1+(1-\rho)^2}} & \text{if } r < r_0, \\ 0 & \text{else,} \end{cases} \qquad \rho = \left(\frac{r}{r_0}\right)^2. \tag{35}$$

As for the previous examples, though being all these vortexes suited for testing high order methods, as they are C^∞, the amplitude of their derivatives changes considerably. To assess this information we plot for various vortexes the profile of $h(r)$ and of $u_\theta(r)$ and their derivatives (up to the 5th derivative). We fix for all the vortexes $r_0 = 1$, the values $h_0 = 1$ and $h(0) = 0.99$, by setting Γ and $g = 1$. In figs. 5 and 6 we plot the vortexes of type (32) for variables h and u_θ respectively, while in figs. 7 and 8 we plot the vortexes for (34).

With the C^∞ vortexes (32) and (34), the profile of h grows to h_0 more slowly, see fig. 5, but the high derivatives are larger with respect to the ones of the previous examples, but they do not vary much with respect to the parameter p. Also for u_θ we observe similar behaviors: comparing the 5th derivatives of these vortexes with the previous ones, we have values at least 100 times larger. With the arctan test cases we actually can slightly decrease the amplitude of high derivatives for large p, as shown in fig. 8.

11

Figure 5: h profile and its derivatives for vortexes (32) with $p = 2, \ldots, 4$

Figure 6: u_θ profile and its derivatives for vortexes (32) with $p = 2, \ldots, 4$

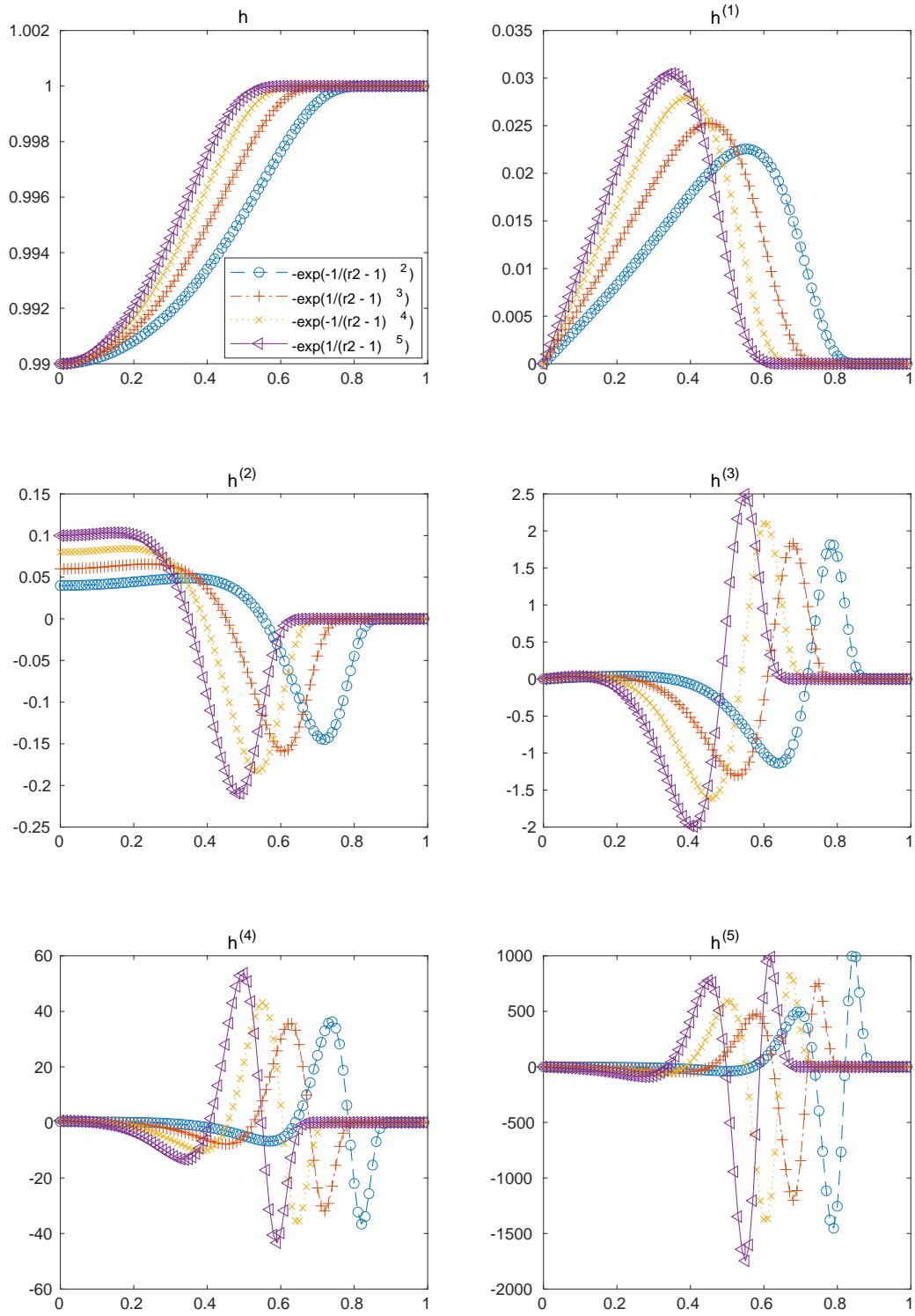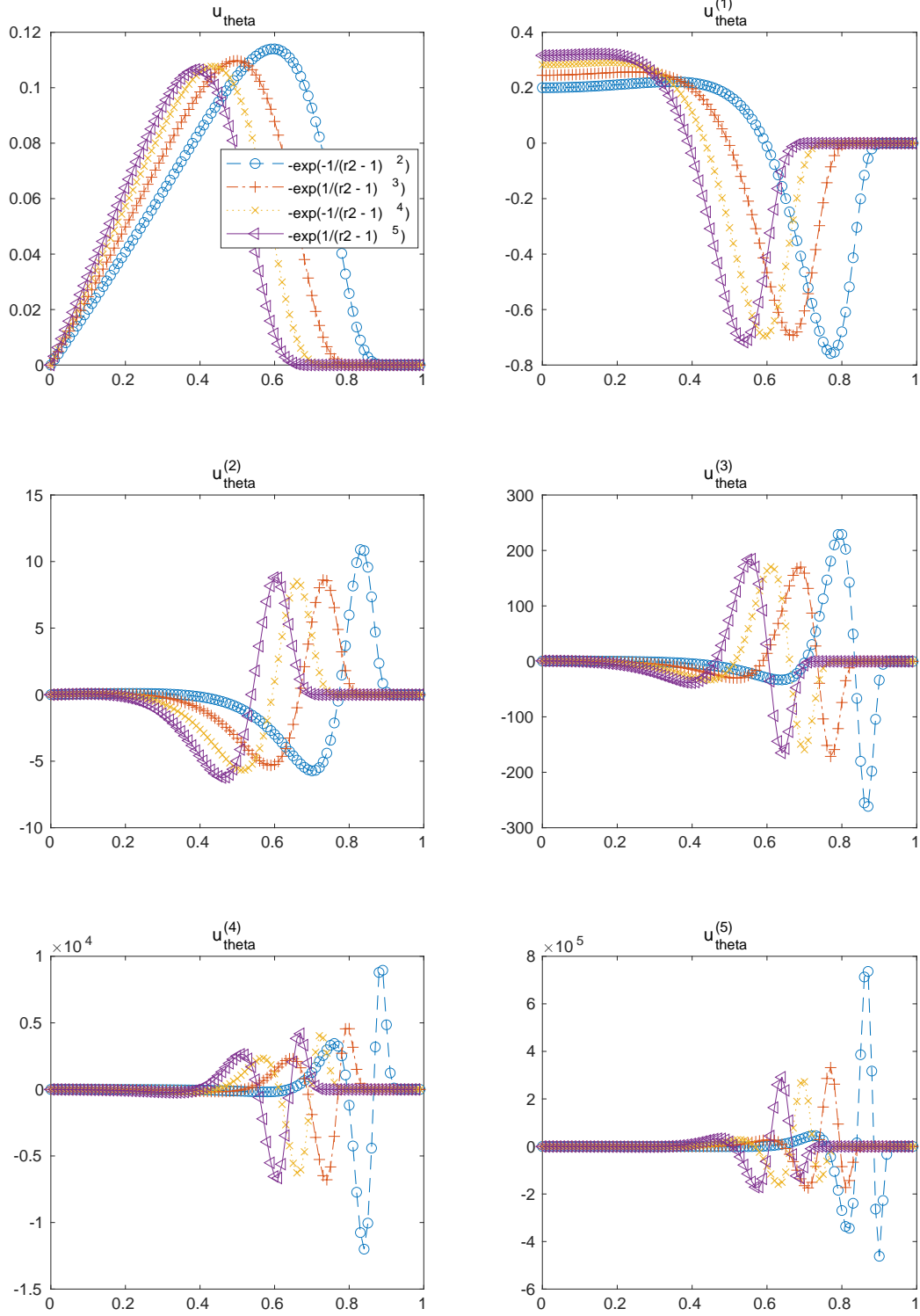Figure 7: h profile and its derivatives for vortexes (34) with $p = 2, \ldots, 4$
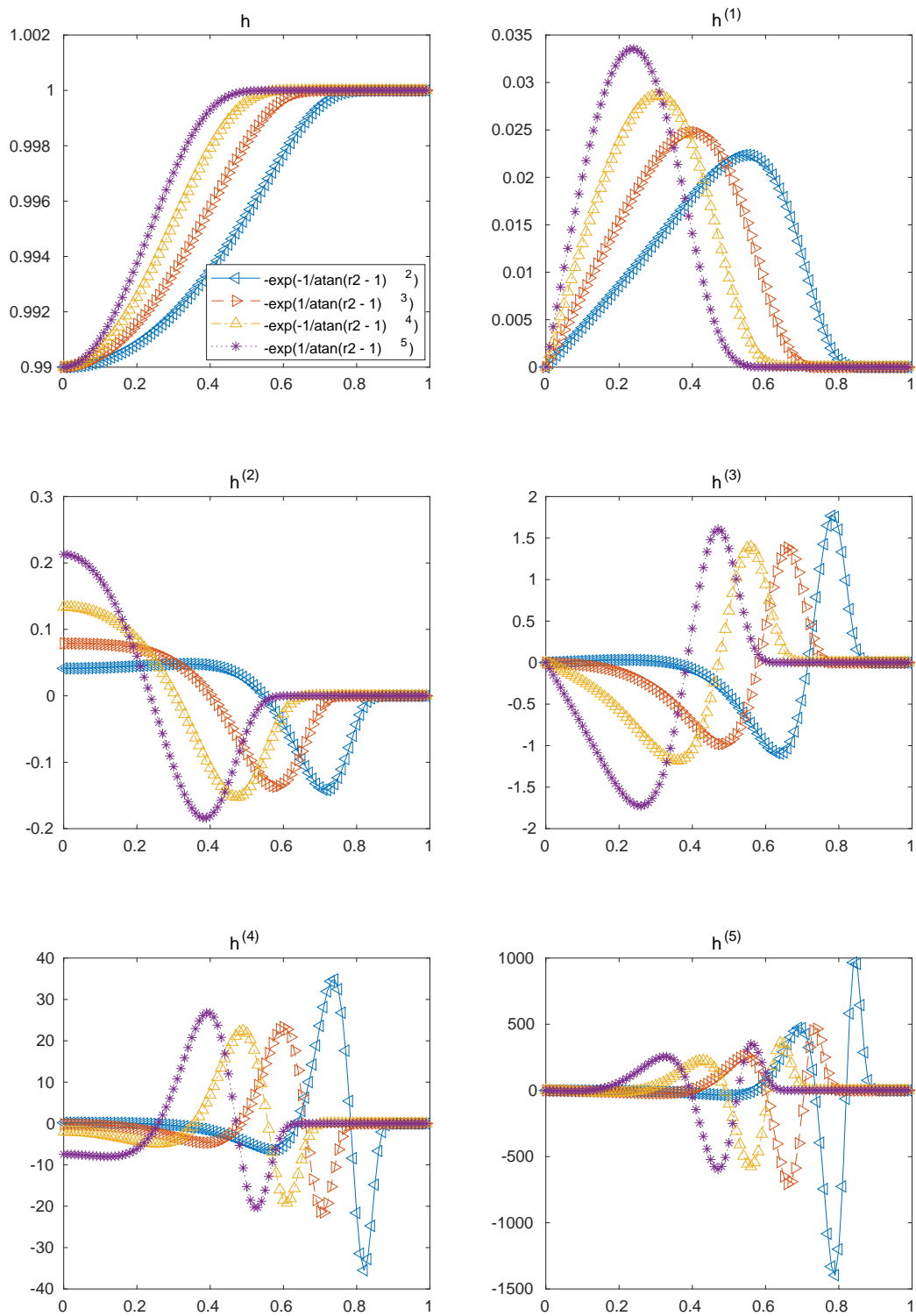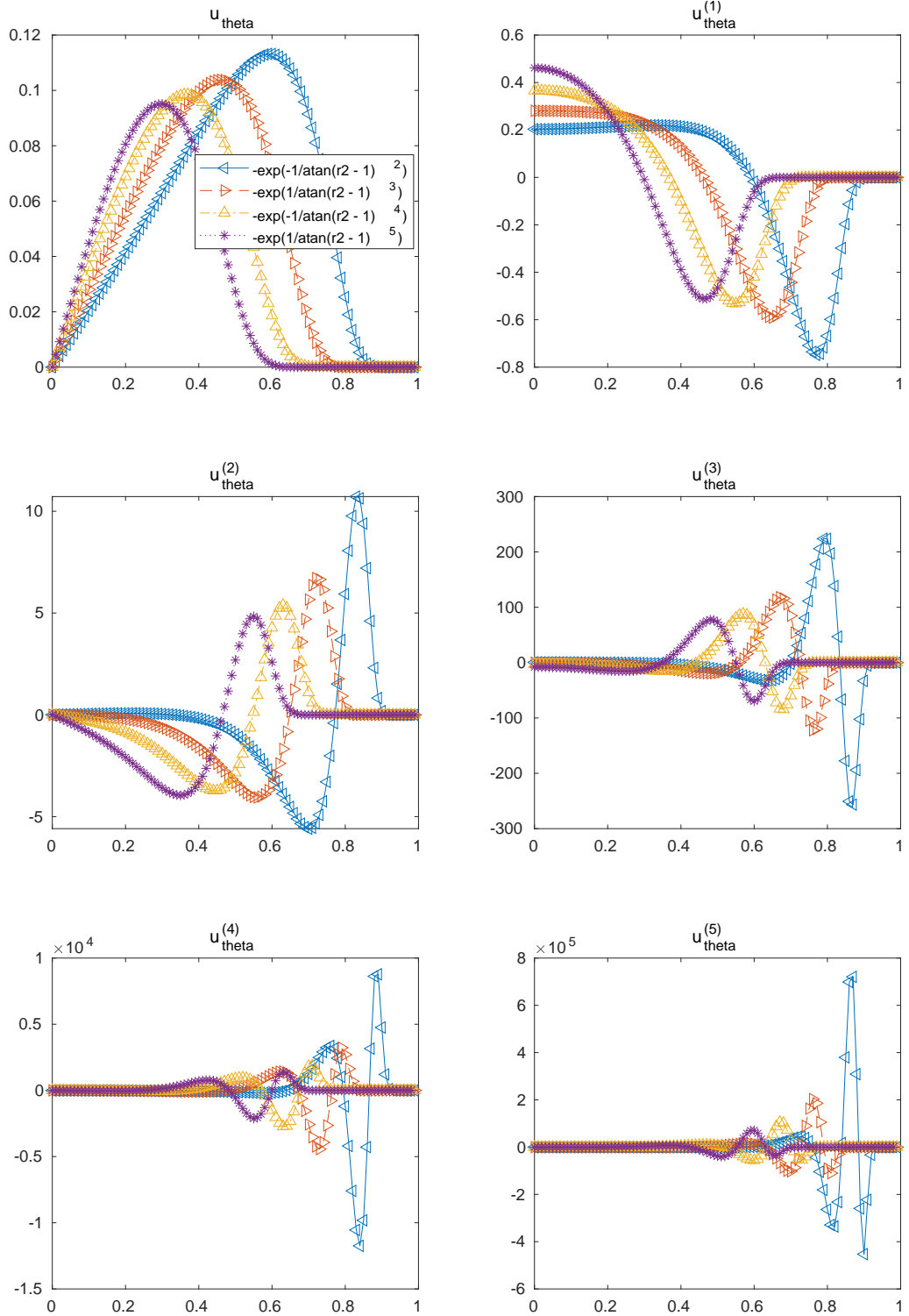
Figure 8: u_θ profile and its derivatives for vortexes (34) with $p = 2, \ldots, 4$

r_0=0.1					
N	Error h	Order h	Error u	Order u	Error v	Order v
25	1.073e-05	0.000	3.078e-04	0.000	3.080e-04	0.000
50	1.537e-06	2.804	3.432e-05	3.165	3.432e-05	3.166
100	5.777e-08	4.734	2.174e-06	3.980	2.174e-06	3.980
200	2.118e-09	4.770	1.045e-07	4.379	1.045e-07	4.379
300	3.081e-10	4.754	1.630e-08	4.581	1.630e-08	4.582
400	7.620e-11	4.857	4.354e-09	4.589	4.354e-09	4.589
500	2.632e-11	4.765	1.568e-09	4.575	1.568e-09	4.576
600	1.198e-11	4.315	6.819e-10	4.569	6.819e-10	4.568
r_0=0.15					
N	Error h	Order h	Error u	Order u	Error v	Order v
25	1.014e-05	0.000	1.804e-04	0.000	1.804e-04	0.000
50	4.589e-07	4.466	1.336e-05	3.755	1.336e-05	3.755
100	1.641e-08	4.806	7.597e-07	4.136	7.597e-07	4.136
200	7.739e-10	4.406	4.224e-08	4.169	4.224e-08	4.169
300	3.228e-10	2.156	1.373e-08	2.772	1.373e-08	2.772
400	2.025e-10	1.622	8.477e-09	1.676	8.477e-09	1.675
500	1.467e-10	1.442	6.465e-09	1.215	6.465e-09	1.215
600	1.127e-10	1.447	5.399e-09	0.988	5.399e-09	0.988
r_0=0.2					
N	Error h	Order h	Error u	Order u	Error v	Order v
25	3.422e-06	0.000	7.886e-05	0.000	7.886e-05	0.000
50	2.184e-07	3.970	9.671e-06	3.028	9.671e-06	3.028
100	9.568e-08	1.190	2.710e-06	1.835	2.710e-06	1.835
200	4.185e-08	1.193	1.467e-06	0.885	1.467e-06	0.885
300	2.465e-08	1.306	1.062e-06	0.798	1.062e-06	0.798
400	1.679e-08	1.333	8.468e-07	0.786	8.468e-07	0.786
500	1.241e-08	1.356	7.097e-07	0.791	7.097e-07	0.791
600	9.701e-09	1.351	6.143e-07	0.792	6.143e-07	0.792

Table 2: Order of convergence for (21) with $r_0 = 0.1, 0.15, 0.2$ obtained with WENO5 on $[0,1]^2$ with a cartesian grid with $N \times N$ cells

5   Numerical tests

We test a 5th order method with the presented vortexes. The method consists of a finite volume discretization on a Cartesian grid with WENO5 reconstruction and Rusanov numerical flux. We use 4 Gauss-Legendre points for one-dimensional quadrature rules. The time discretization is carried out with Butcher's RK(6,5) 6 stages 5th order method, see appendix B for its Butcher's tableau. The CFL number used is 0.95. The domain is $[0,1]^2$ and it is discretized with uniform Cartesian grids and periodic boundary conditions. The vortexes are set with $h_0 = 1$, $h_{min} = 0.99$ and $r_0 = 0.45$, while for the non compact supported one we test different r_0 parameters. Final time is set to $T = 1$, but it might be useful to run the code for larger or smaller times. In [8] it is well observed how this impact on the convergence of the method as the machine precision error accumulates exponentially in time, one might see its effect before reaching the desired accuracy. On the other side, small final time T leads to very small errors also for coarser meshes, not letting appreciate the quality of the high order schemes.

   With the non compact supported vortex we obtain the results in table 2. We observe for large values of r_0 that the error from the boundary effect is predominant already for very coarse meshes. For $r_0 = 0.2$ (corresponding to $r_0 = 0.4$ in figs. 1 and 2) we have a discontinuity of the order of 10^{-6} for the velocity

			p=1			
N	Error h	Order h	Error u	Order u	Error v	Order v
25	1.767e-04	0.000	1.477e-03	0.000	1.477e-03	0.000
50	1.716e-05	3.365	2.420e-04	2.610	2.420e-04	2.610
100	1.409e-06	3.606	4.610e-05	2.392	4.610e-05	2.392
200	1.367e-07	3.366	9.036e-06	2.351	9.036e-06	2.351
300	3.817e-08	3.147	3.416e-06	2.399	3.416e-06	2.399
400	1.576e-08	3.076	1.705e-06	2.416	1.705e-06	2.416
500	7.966e-09	3.056	9.942e-07	2.416	9.942e-07	2.416
600	4.568e-09	3.050	6.415e-07	2.403	6.415e-07	2.403

			p=2			
N	Error h	Order h	Error u	Order u	Error v	Order v
25	2.072e-04	0.000	1.615e-03	0.000	1.614e-03	0.000
50	2.274e-05	3.188	1.827e-04	3.144	1.827e-04	3.144
100	9.111e-07	4.641	1.717e-05	3.411	1.717e-05	3.411
200	3.305e-08	4.785	1.136e-06	3.918	1.136e-06	3.918
300	4.701e-09	4.810	2.215e-07	4.031	2.215e-07	4.031
400	1.207e-09	4.725	6.977e-08	4.016	6.977e-08	4.016
500	4.413e-10	4.511	2.870e-08	3.981	2.870e-08	3.981
600	2.091e-10	4.096	1.392e-08	3.966	1.393e-08	3.966

			p=3			
N	Error h	Order h	Error u	Order u	Error v	Order v
25	1.684e-04	0.000	1.471e-03	0.000	1.471e-03	0.000
50	3.635e-05	2.212	2.538e-04	2.536	2.537e-04	2.536
100	1.598e-06	4.508	1.944e-05	3.706	1.944e-05	3.706
200	5.794e-08	4.786	8.602e-07	4.498	8.603e-07	4.498
300	7.942e-09	4.901	1.240e-07	4.777	1.240e-07	4.778
400	1.938e-09	4.903	3.176e-08	4.735	3.176e-08	4.734
500	6.658e-10	4.788	1.105e-08	4.732	1.105e-08	4.732
600	2.958e-10	4.450	4.626e-09	4.775	4.626e-09	4.775

Table 3: Order of convergence for (25) with $p = 1, \ldots, 3$ obtained with WENO5 on a cartesian grid with $N \times N$ cells

variables on the boundary of the domain (periodic BCs) and this prevent reaching more than 3rd order in the coarse regime. For $r_0 = 0.15$ we see again boundary effects but for finer meshes, hence it is possible to reach an order of accuracy 4 for few steps in the mesh refinement process. On the other side, we have for $r_0 = 0.1$ (corresponding to $r_0 = 0.2$ in figs. 1 and 2) that h at the boundaries is 1 up to machine precision and $u_\theta \approx 10^{-12}$. Indeed, the convergence in this test is smooth enough for $T = 1$, even for not too fine meshes. Nevertheless, one should really be careful using this vortex in hitting machine precision at the boundaries.

For the tests run with the cos vortexes (25), we observe that for $p = 1$ we reach order 3 for h and around 2.4 for u, a little better than expected, for $p = 2$ the order reaches 4 and almost 5 for h, and finally for $p = 3$ we essentially obtain the expected 5th order of the scheme already at the mesh 300×300.

For the C^∞ cases we observe that a finer mesh is needed to reach the expected accuracy, in particular for the (32) tests, where we barely reach it for u with the mesh with $N = 600$. We observe in this case that we obtain better convergence orders for smaller times, e.g. $T = 0.1$.

In the arctan vortex (34) we have smaller amplitude of higher derivatives, in particular for large p, so with $p = 3, 4$ we see an order of accuracy larger than 4 for $N = 600$, which is a bit better than with the only exponential test, still with a quite fine mesh. The same reasoning holds for these tests and with

			p=2			
N	Error h	Order h	Error u	Order u	Error v	Order v
25	3.367e-04	0.000	2.965e-03	0.000	2.966e-03	0.000
50	1.301e-04	1.372	1.239e-03	1.258	1.239e-03	1.259
100	3.142e-05	2.050	3.213e-04	1.948	3.213e-04	1.948
200	3.005e-06	3.387	5.399e-05	2.573	5.399e-05	2.573
300	5.146e-07	4.352	1.387e-05	3.353	1.387e-05	3.353
400	1.205e-07	5.045	5.169e-06	3.430	5.169e-06	3.430
500	3.715e-08	5.275	2.542e-06	3.181	2.542e-06	3.181
600	1.427e-08	5.247	1.362e-06	3.420	1.362e-06	3.420

			p=3			
N	Error h	Order h	Error u	Order u	Error v	Order v
25	3.186e-04	0.000	2.459e-03	0.000	2.459e-03	0.000
50	1.092e-04	1.544	1.017e-03	1.273	1.017e-03	1.273
100	2.372e-05	2.203	2.401e-04	2.083	2.401e-04	2.083
200	1.815e-06	3.708	3.212e-05	2.902	3.212e-05	2.902
300	2.577e-07	4.815	7.621e-06	3.548	7.621e-06	3.548
400	5.728e-08	5.227	2.966e-06	3.281	2.966e-06	3.281
500	1.810e-08	5.162	1.339e-06	3.565	1.339e-06	3.565
600	7.234e-09	5.030	6.317e-07	4.119	6.317e-07	4.119

			p=4			
N	Error h	Order h	Error u	Order u	Error v	Order v
25	3.047e-04	0.000	2.424e-03	0.000	2.425e-03	0.000
50	1.016e-04	1.584	9.224e-04	1.394	9.224e-04	1.394
100	2.232e-05	2.187	2.205e-04	2.065	2.205e-04	2.065
200	1.657e-06	3.752	2.706e-05	3.027	2.706e-05	3.027
300	2.273e-07	4.899	6.324e-06	3.585	6.324e-06	3.585
400	5.102e-08	5.194	2.485e-06	3.247	2.485e-06	3.247
500	1.639e-08	5.089	1.075e-06	3.755	1.075e-06	3.755
600	6.636e-09	4.959	4.934e-07	4.272	4.934e-07	4.272

			p=5			
N	Error h	Order h	Error u	Order u	Error v	Order v
25	2.920e-04	0.000	2.256e-03	0.000	2.255e-03	0.000
50	1.002e-04	1.543	9.002e-04	1.325	9.002e-04	1.325
100	2.275e-05	2.139	2.180e-04	2.046	2.180e-04	2.046
200	1.749e-06	3.701	2.608e-05	3.064	2.608e-05	3.064
300	2.413e-07	4.886	6.022e-06	3.615	6.021e-06	3.615
400	5.463e-08	5.164	2.383e-06	3.222	2.383e-06	3.222
500	1.766e-08	5.060	1.027e-06	3.771	1.027e-06	3.770
600	7.171e-09	4.944	4.691e-07	4.300	4.691e-07	4.300

Table 4: Order of convergence for (32) with $p = 2, \ldots, 5$ obtained with WENO5 on a cartesian grid with $N \times N$ cells

p=2						
N	Error h	Order h	Error u	Order u	Error v	Order v
25	3.315e-04	0.000	2.935e-03	0.000	2.935e-03	0.000
50	1.271e-04	1.383	1.216e-03	1.271	1.216e-03	1.272
100	3.040e-05	2.064	3.141e-04	1.952	3.141e-04	1.952
200	2.895e-06	3.392	5.286e-05	2.571	5.286e-05	2.571
300	4.950e-07	4.356	1.358e-05	3.352	1.358e-05	3.352
400	1.160e-07	5.044	5.067e-06	3.426	5.067e-06	3.426
500	3.579e-08	5.269	2.492e-06	3.180	2.492e-06	3.180
600	1.377e-08	5.239	1.335e-06	3.424	1.335e-06	3.424

p=3						
N	Error h	Order h	Error u	Order u	Error v	Order v
25	2.897e-04	0.000	2.259e-03	0.000	2.259e-03	0.000
50	8.398e-05	1.787	8.381e-04	1.431	8.381e-04	1.430
100	1.536e-05	2.451	1.734e-04	2.273	1.734e-04	2.273
200	1.040e-06	3.884	2.194e-05	2.982	2.194e-05	2.982
300	1.412e-07	4.925	5.295e-06	3.506	5.295e-06	3.506
400	3.214e-08	5.146	2.072e-06	3.262	2.072e-06	3.262
500	1.036e-08	5.074	8.860e-07	3.806	8.860e-07	3.806
600	4.199e-09	4.952	4.054e-07	4.288	4.054e-07	4.288

p=4						
N	Error h	Order h	Error u	Order u	Error v	Order v
25	2.637e-04	0.000	2.123e-03	0.000	2.123e-03	0.000
50	6.696e-05	1.978	6.581e-04	1.690	6.581e-04	1.690
100	1.052e-05	2.670	1.210e-04	2.444	1.210e-04	2.444
200	5.934e-07	4.148	1.284e-05	3.236	1.284e-05	3.235
300	7.766e-08	5.015	3.256e-06	3.385	3.256e-06	3.384
400	1.812e-08	5.059	1.156e-06	3.601	1.156e-06	3.601
500	6.034e-09	4.928	4.470e-07	4.257	4.470e-07	4.257
600	2.515e-09	4.799	1.982e-07	4.461	1.982e-07	4.461

p=5						
N	Error h	Order h	Error u	Order u	Error v	Order v
25	2.020e-04	0.000	1.739e-03	0.000	1.739e-03	0.000
50	6.518e-05	1.632	5.841e-04	1.574	5.841e-04	1.574
100	8.822e-06	2.885	9.722e-05	2.587	9.721e-05	2.587
200	4.440e-07	4.312	8.910e-06	3.448	8.909e-06	3.448
300	5.833e-08	5.006	2.335e-06	3.302	2.335e-06	3.302
400	1.396e-08	4.972	7.587e-07	3.908	7.587e-07	3.908
500	4.712e-09	4.866	2.826e-07	4.425	2.826e-07	4.425
600	1.972e-09	4.776	1.250e-07	4.476	1.250e-07	4.476

Table 5: Order of convergence for (34) with $p = 2, \ldots, 5$ obtained with WENO5 on a cartesian grid with $N \times N$ cells

smaller final times we can observe better convergence order (around 4.8 for $p \geq 3$).

6 Conclusion

Steady and moving vortex solutions are useful tools to test the order of accuracy of high order methods for hyperbolic balance laws (shallow water and Euler equations). The vortexes known in literature are, anyway, either discontinuous in some derivatives [6], hence not suitable for very high order methods, or non compact supported [7], hence presenting troubles with boundary conditions if the parameters are not carefully chosen.

In this work we propose a class of $\mathcal{C}^{2p}$ compactly supported vortexes with arbitrary p, and some $\mathcal{C}^{\infty}$ compactly supported vortexes. The latter are very attractive as they do not need to compute integrals, but only derivatives, and have all the derivatives continuous. On the other side, their derivatives are particularly large and the expected order of accuracy is reached only for very fine meshes. The one that obtain better results in this class is the one based on the arctan with $p = 5$ for final time $T = 0.1$. For larger times the order is not so neat.

Among the cos based vortexes, the one with $p = 3$ gives better results (for order 5 schemes) even for coarser meshes $N_x \approx 300$, as its derivative are not too large. On the other side, this vortex can only be used to test methods up to order 6 of accuracy.

Overall, we suggest the use of $\mathcal{C}^{\infty}$ vortexes for testing arbitrarily high order methods, while, for a fixed method of order $d \leq 2p$ the recipe (25) builds a vortex where the order of accuracy can be observed in coarser meshes.

Acknowledgments

A Values of H_p

Here, we provide the explicit form of H_p for $p = 1, \ldots, 3$, the corresponding h can be computed from (25). The value of Γ can be set given h_{min}, using

$$\Gamma = \frac{\pi}{2^p r_0} \sqrt{\frac{g(h_0 - h_{min})}{H_p(\pi/2) - H_p(0)}}. \tag{36}$$

We provide in the following also the value of $H_p(\pi/2) - H_p(0)$.

$$H_1(x) = \frac{\cos(2x)}{8} + \frac{x\sin(2x)}{4} + \frac{\cos(2x)^2}{64} + \frac{3x^2}{16} + \frac{x\cos(2x)\sin(2x)}{16},$$

$$H_1(\pi/2) - H_1(0) = \frac{3\pi^2}{64} - \frac{1}{4},$$

$$H_2(x) = \frac{35\cos(2x)}{384} + \frac{35x\sin(2x)}{192} + \cos(x)^6\left(\frac{\cos(x)^2}{64} + \frac{7}{288}\right) + \frac{35\cos(2x)^2}{3072} +$$

$$\frac{35x^2}{256} + \frac{35x\cos(2x)\sin(2x)}{768} + \frac{x\cos(x)^5\sin(x)(\cos(x)^2 + 7/6)}{8},$$

$$H_2(\pi/2) - H_2(0) = \frac{35\pi^2}{1024} - \frac{2}{9},$$

20

$$H_3(x) = \frac{77\cos(2x)}{1024} + \frac{77x\sin(2x)}{512} + \frac{33\cos(x)^6(\cos(x)^2/64 + 7/288)}{40} + \cos(x)^{10}\left(\frac{\cos(x)^2}{144} + \frac{11}{1200}\right) +$$

$$\frac{77\cos(2x)^2}{8192} + \frac{231x^2}{2048} + \frac{77x\cos(2x)\sin(2x)}{2048} + \frac{33x\cos(x)^5\sin(x)(\cos(x)^2 + 7/6)}{320} +$$

$$\frac{x\cos(x)^9\sin(x)(\cos(x)^2 + 11/10)}{12},$$

$$H_3(\pi/2) - H_3(0) = \frac{231\pi^2}{8192} - \frac{359}{1800}.$$

B   Runge Kutta (6,5)

The Butcher Tableau of Butcher's Runge Kutta (6,5) method used is the following

$$
\begin{array}{c|cccccc}
0 & & & & & & \\
\frac{1}{4} & \frac{1}{4} & & & & & \\
\frac{1}{4} & \frac{1}{8} & \frac{1}{8} & & & & \\
\frac{1}{2} & 0 & 0 & \frac{1}{2} & & & \\
\frac{3}{4} & \frac{3}{16} & -\frac{3}{8} & \frac{3}{8} & \frac{9}{16} & & \\
1 & -\frac{3}{7} & \frac{8}{7} & \frac{6}{7} & -\frac{12}{7} & \frac{8}{7} & \\
\hline
 & \frac{7}{90} & 0 & \frac{16}{45} & \frac{2}{15} & \frac{16}{45} & \frac{7}{90}
\end{array}
. \tag{37}
$$

References

[1] R. Abgrall, P. Bacigaluppi, and S. Tokareva, *High-order residual distribution scheme for the time-dependent Euler equations of fluid dynamics*, Computers & Mathematics with Applications, 78 (2019), pp. 274–297.

[2] R. Abgrall and D. Torlo, *High order asymptotic preserving deferred correction implicit-explicit schemes for kinetic models*, SIAM Journal on Scientific Computing, 42 (2020), pp. B816–B845.

[3] A. Ern and J.-L. Guermond, *Theory and practice of finite elements*, vol. 159, Springer Science & Business Media, 2013.

[4] L. Euler, *Principes généraux du mouvement des fluides*, Académie Royale des Sciences et des Belles Lettres de Berlin, Mémoires (1755), pp. 274–315.

[5] J. S. Hesthaven and T. Warburton, *Nodal discontinuous Galerkin methods: algorithms, analysis, and applications*, Springer Science & Business Media, 2007.

[6] M. Ricchiuto and A. Bollermann, *Stabilized residual distribution for shallow water simulations*, Journal of Computational Physics, 228 (2009), pp. 1071–1115.

[7] C.-W. Shu, *Essentially non-oscillatory and weighted essentially non-oscillatory schemes for hyperbolic conservation laws*, in Advanced numerical approximation of nonlinear hyperbolic equations, Springer, 1998, pp. 325–432.

[8] S. C. Spiegel, H. Huynh, and J. R. DeBonis, *A survey of the isentropic Euler vortex problem using high-order methods*, in 22nd AIAA Computational Fluid Dynamics Conference, 2015, p. 2444.

[9] Z. J. Wang and H. Gao, *A unifying lifting collocation penalty formulation including the discontinuous galerkin, spectral volume/difference methods for conservation laws on mixed grids*, Journal of Computational Physics, 228 (2009), pp. 8161–8186.

[10] Z. J. Wang, Y. Liu, G. May, and A. Jameson, *Spectral difference method for unstructured grids ii: extension to the Euler equations*, Journal of Scientific Computing, 32 (2007), pp. 45–71.